45th AIAA Aerospace Sciences Meeting and Exhibit, January 8-11, 2007, Reno, NV

Validation of Blockage Interference Corrections in the National Transonic Facility (Invited)

Eric L. Walker*
NASA Langley Research Center, Hampton, VA 23681

A validation test has recently been constructed for wall interference methods as applied to the National Transonic Facility (NTF). The goal of this study was to begin to address the uncertainty of wall-induced-blockage interference corrections, which will make it possible to address the overall quality of data generated by the facility. The validation test itself is not specific to any particular modeling. For this present effort, the Transonic Wall Interference Correction System (TWICS) as implemented at the NTF is the mathematical model being tested. TWICS uses linear, potential boundary conditions that must first be calibrated. These boundary conditions include three different classical, linear, homogeneous forms that have been historically used to approximate the physical behavior of longitudinally slotted test section walls. Results of the application of the calibrated wall boundary conditions are discussed in the context of the validation test.

Nomenclature

A	Area
B	Porosity Parameter
C	Test section cross-sectional area
C_D	Drag coefficient
$\bar{C}_D$	Average drag coefficient
d	Diameter
GSW	General Slotted Wall
ISW	Ideal Slotted Wall
K	Slotted Wall Parameter
L	Length
M	Mach number
PW	Porous Wall
p_0	Total pressure
q	Dynamic pressure
S	Reference area
U	Velocity
u, v, w	Velocity perturbation; x, y, z component
V	Volume
x, y, z	Cartesian axes
β	$\sqrt{1-M^2}$
Δ	Correction
ε	Blockage
$\hat{\sigma}$	Estimate of the standard deviation
ϕ	Perturbation velocity potential
φ	Interference velocity potential
χ	System Response Quantity

Subscripts

∞	Corrected free stream quantity
c	Corrected
cav	Cavity
etb	Empty test section buoyancy
f	Test article in free-air
fit	Computational fit by TWICS
i	Interference
m	Measured
meas	Measured
mib	Solid blockage induced buoyancy
t	Test article in tunnel
T	Tared
TS	Test Section
u	Uncorrected for wall interference
w	Wall interference induced

*Research Engineer. Lifetime Member AIAA.

I. Introduction

Current trends in wind tunnel testing of aerodynamic vehicles are of increasingly larger test articles in relatively small test sections. This trend appears to be driven by cost and fidelity requirements of customers of the resulting data. Smaller test sections decrease overhead costs with respect to those of larger facilities. Larger test articles increase the geometric fidelity of the represented vehicle. This trend of a shrinking test section with respect to the test article results in increased wall interference effects on the aerodynamics of the represented vehicle. In some cases, this can place the test article in a flow field that is so unrealistic that there is no corresponding free-air or unbounded flight equivalent—hence, yielding an uncorrectable situation.

In recent years, much more emphasis has been placed on uncertainty quantification of data. Most work in the area of uncertainty quantification is targeted toward understanding dispersion seen in the data. This observed dispersion is an important component of the total uncertainty; however, an equally important but more difficult to obtain component of the total uncertainty is that due to systematic errors in the mathematical modeling (epistemic uncertainty) of corrections made to the data. In 2001, a study was initiated at the NASA Langley Research Center (LaRC) National Transonic Facility (NTF) to characterize the epistemic uncertainty of wall corrections as applied to a longitudinally slotted test section. An overview of the plan devised to analyze the effect of wall interference by explicitly changing the level of the interference on a test article was presented by Walker[1] in 2004. The plan, as presented, covered both blockage and lift interference effects. The first portion of this plan, covering calibration and validation of blockage interference corrections, was completed in late 2005 and documented by Walker.[2, 3]

The context for this body of work was three-fold. First, it is a critical step in a data quality assurance program underway at NASA LaRC.[4, 5] It is essential to understand the uncertainty in each element of a reported quantity to properly quantify the uncertainty associated with that quantity. This is demonstrated using C_D as shown below in Equation 1:

$$\left.\begin{array}{l} C_{D_c} = C_{D_m} + \Delta C_{D_w} + \cdots \\ \hat{\sigma}^2_{C_{D_c}} = \hat{\sigma}^2_{C_{D_m}} + \hat{\sigma}^2_{\Delta C_{D_w}} + \cdots \end{array}\right\} C_{D_c} \pm \hat{\sigma}_{C_{D_c}} \tag{1}$$

where $\hat{\sigma}^2$ represents the variance of the respective terms in the drag coefficient correction equation. Corrections are often applied to data, but the uncertainty of these corrections is often unknown or not well understood. Neglection of the correction uncertainties can grossly effect the total uncertainty of the corrected quantity.

Second, it will help determine where the correction methods are applicable. Determining where the model no longer adequately predicts the free-air response allows boundaries and criteria to be established for proper use of the method. This also allows the quality of wall interference correction method to be measured.

Third, this work will allow for decisions to be made concerning wall correction modeling improvements, enabling constrained resources to be focused on minimizing the largest uncertainties; thus, providing a way to assess extensions of the modeling beyond its originally intended application.

The purpose of this paper is to provide a summary of the development of a validation process and its application to blockage interference corrections at the NTF. First, the validation test for wall-induced-blockage interference is constructed. This is followed by a mathematical model discrimination and validation analysis of the calibrated wall boundary condition models for the NTF. A summary is given to conclude the paper.

II. Constructing a Validation Test For Wall-Induced-Blockage Interference

The purpose of this section is to discuss aspects of establishing a validation test within the context of the present study—wall-induced-blockage interference. Experimentation required for the validation test is presented and the results are discussed. The framework of the validation test discussed below is independent of the selection of the wall interference wall interference model, and as such can be used as a test of validity for any future wall interference model that is implemented at the NTF.

Before proceeding with the validation test construction, it is necessary to discuss some background information that will facilitate the development of the validation test for wall interference—namely, a brief introduction to the NTF and TWICS. The elements of the validation test are discussed in the context of

TWICS-NTF application. A summary of the experimental work used for the validation test is presented along with a discussion of the results.

A. Description of the National Transonic Facility

The NTF[6] is a fan-driven, closed-circuit, continuous-flow, pressurized wind tunnel, which is capable of testing at cryogenic conditions. The test gas is dry air for elevated temperature operation and nitrogen for reduced temperature operation. The settling chamber contains four anti-turbulence screens. A 15:1 contraction ratio entrance cone leads into an 8.2 feet square cross-sectional test section with 6 inch triangular corner fillets. The test section extends 25 feet in length, of which 6 feet constitutes the calibrated test section, then opens into a high speed diffuser. The operational envelope of the NTF encompasses a large range of test conditions. The facility can sustain a continuous airspeed from 0.1 to 1.2 in Mach number. Total pressure capabilities of the facility range from 15 to 130 psi. The tunnel can operate at temperatures ranging from $150°F$ down to $-320°F$. These large ranges of conditions allow for unit Reynolds number testing from 3 to 120 million per foot. NTF has the capability to independently vary Mach number, Reynolds number, and dynamic pressure.

Currently, the NTF has 459 operational wall pressure orifices of which the NTF-TWICS code uses up to 360. Figure 1 shows the wall pressure orifice layout in the test section. The orifices are displayed in context of the major features of the test section: the slots in the floor and ceiling and the reentry flaps at the rear of the test section. Also displayed is the center of rotation at tunnel station 13 feet.

B. Transonic Wall Interference Correction System (TWICS)

TWICS and its predecessor the Wall Interference Correction System (WICS) were developed at the NASA Ames Research Center by Ulbrich *et al.*[7–14] as a modification and extension of the Hackett wall signature method.[15–22] TWICS is an enhanced version of WICS that handles ventilated boundary conditions, typically seen in transonic wind tunnels. This method was chosen to be implemented at two facilities at the NASA LaRC, see Iyer *et al.*,[23,24] in an effort to standardize the wall interference correction methodology across NASA centers. TWICS is a linear potential based method which inherently assumes that there is a portion of flow in the test section between the near-field region of the test article and the near-field region of the wall that is a linear perturbation of the empty test section flow field and governed by

$$\beta^2\phi_{xx} + \phi_{yy} + \phi_{zz} = 0 \tag{2}$$

where $\beta^2 = 1 - M^2$, ϕ is the perturbation velocity potential, and M is the free-stream Mach number. Since it is a linear potential method based on a Prandtl-Glauert compressibility model, the TWICS modeling is not expected to work well at transonic conditions, where the assumption of subcritical flow at the wall is violated. One of the aspects of the validation testing structure to be discussed is to determine where the method remains applicable (*i.e.,* how high in Mach number can the method be used) and the consequences of using the method (*i.e.,* how much uncertainty filters into C_D).

The method uses a tared wall pressure signature, which is the difference between the model installed condition and the empty test section, a database of normalized perturbation velocities using unit singularity solutions computed for a given mathematical representation of the wall boundary condition, and geometric information from the test article. Tareing of the wall pressure signature is performed to remove first order effects of the empty tunnel boundary layer and buoyancy, is assumed to contain only the solid and wake blockage, and is also assumed that the additional second order change in the test-section-wall boundary layer displacement thickness due to the presence of the test article is negligible—an assumption that is violated by flow near a Mach number of unity where aspects of the crossflow are more critical. The test article is modeled with an appropriately weighted point doublet chain[25] to represent the fuselage, wake, and support system.

For the present study, normalized perturbation velocities are calculated using the method of Pindzola and Lo[26] for the unit point-doublet singularities with a specified wall boundary condition. The following equations represent the available linearized homogeneous wall boundary conditions presently available for TWICS-NTF.

$$\varphi_x + K\varphi_{xn} + B\varphi_n = 0 \qquad \text{General Slotted Wall (GSW)} \tag{3}$$

$$\varphi_x + K\varphi_{xn} = 0 \qquad \text{Ideal Slotted Wall (ISW)} \tag{4}$$

$$\varphi_x + B\varphi_n = 0 \qquad \text{Porous Wall (PW)} \tag{5}$$

$$\varphi_x = 0 \qquad \text{Open Jet} \tag{6}$$

$$\varphi_n = 0 \qquad \text{Solid Wall} \tag{7}$$

where $\varphi \approx \phi_t - \phi_f$ is the interference velocity potential, ϕ_t is the perturbation velocity potential of the test article in the test section, ϕ_f is the perturbation velocity potential of the test article in an unconstrained flow field (free air), K is the slotted wall parameter, and B is the porosity parameter. Equation 3, denoted General Slotted Wall (GSW), is the most general linear form of the boundary condition currently available for use in the TWICS code. This boundary condition has been shown by Everhart[27] to be the result of linearizing the non-linear slotted wall boundary condition, and it states that the pressure at the wall (from φ_x term) is a balance of the streamline curvature at the wall (from φ_{xn} term) and the pressure drop across the wall (from φ_n term). The other four boundary conditions given in Equations 4-7 are obtained by setting the parameters, K, B in Equation 3, to appropriate values. For the Ideal Slotted Wall boundary condition (ISW), given in Equation 4, $B = 0$, indicating that the pressure at the wall is solely determined by the streamline curvature at the wall. For the Porous Wall boundary condition (PW), given in Equation 5, $K = 0$, indicating that the pressure at the wall is solely determined by the pressure drop across the wall. The Open Jet (Equation 6) and Solid Wall (Equation 7) boundary condition are obtained by setting $K = B = 0$ and $K \to \infty$ or $B \to \infty$, respectively. Historically, three ventilated wall boundary conditions (Equations 3-5) have been used to approximate the physical behavior at a slotted wall. Attempts to relate the parameters, K, B, to geometrical properties of the test section have failed, requiring that the values of these parameters be determined by detailed measurements or by a calibration procedure. Due to the sizable resource allocation required for the detailed measurements, an indirect approach to calibration of these parameters was devised and executed by Walker.[2,3] Also discussed by Walker is the disagreement among practitioners as to which of these wall boundary conditions is most appropriate for longitudinally slotted walls; therefore, a discrimination analysis is conducted along with the validation analysis to demonstrate which of the three boundary conditions is the most appropriate.

Using the tared wall signature, the database of normalized perturbation velocities for a given wall boundary condition, and the test-article singularity model, the strengths of the singularities representing solid and wake blockage are determined as a result of a global least squares fit. The interference velocity field is then determined by superimposing these singularities with their corresponding calculated strengths; thus allowing the blockage and solid-blockage-induced buoyancy to be determined. The blockage interference factor ε is defined by

$$\varepsilon = \frac{u_i}{U_{\mathrm{TS}}} \approx \frac{u_t - u_f}{U_{\mathrm{TS}}} \tag{8}$$

where $u_i/U_{\mathrm{TS}} = \partial\varphi/\partial x$ is the normalized, axial, interference perturbation velocity, U_{TS} is the test section velocity determined by the facility, and u_t and u_f are the axial perturbation velocities from ϕ_t and ϕ_f, respectively. The solid-blockage-induced buoyancy is the axial gradient of the interference perturbation velocity along the test-article centerline. A more detailed discussion of these calculations is provided by Walker.[2,3]

C. Elements of the Validation Test

As discussed by Walker,[2,3] there are four elements necessary to design a validation test of a given mathematical model:

1. Selection of a Specific Problem of Interest
2. Generation of Independent Cases for Comparison
3. Severe Testing/Placing the Model in Jeopardy of Failure
4. Quantification of Uncertainty

Each of the elements presented above is discussed in the context of the present study and the resulting experimental effort that supplies the data for the mathematical model validation analysis. The experimental

component uses testing strategies similar to those used in the past for wall boundary condition model development and calibration and exploits factors influencing the choice of a wall interference correction method. Instead of model development, however, this study is focused on how well a given math model can correct various situations to free air, and thereby, allow the determination of the method validity and accuracy. The fundamental question is: Can independent cases be established such that, after correction, they yield the same result to within some accuracy? Uncertainties involved in the experimentation required to create these independent cases will establish the basic level of accuracy by which the validity of the correction process will be judged. Any differences seen that are not directly attributable to uncertainty in the measurement process will be assumed to be due to epistemic error of the wall interference model.

Another key element of a validation test is the notion of independence. Care must be taken to ensure that data acquisition, data aggregation, model calibration, etc. be performed in such a way that the independence of cases for validation is not violated. In the context of wall interference, the goal is to select and test several independent cases which, after correction, should yield the same expected result. In other words, a geometric shape should be exposed to different levels of interference that can reasonably be corrected provided the mathematical modeling is adequate. These levels of interference can be generated in the following ways:

1. Geometrically scaling the test article
2. Modification of the physical wall boundary condition
   (a) Using adaptation (*i.e.,* closed walls with deflection capability or active ventilation)
   (b) Using ventilation (*i.e.,* changes to the test section porosity or openness)

Items (1) and (2b) are used to generate the independent cases for use in this present work and are discussed below. Item (2a) is beyond the scope of this present effort, but could be used to construct a validation test in facilities with this capability.

To address item (1) from above, the NTF has a series of three geometrically-scaled, blunt, supercritical bodies of revolution. The two larger bodies, C3 and C4, and their scaled sting supports used in this present effort are shown in Figure 2. These bodies have a fineness ratio of approximately 9.5 and were geometrically-scaled based on test-article volume. The geometry for the NTF bodies are scaled versions from one of the series of bodies of revolution tested in the Langley 16-Foot Transonic Tunnel and the Langley 8-Foot Transonic Pressure Tunnel (8FT) by Couch and Brooks[28] to assess the extent of transonic wall interference effects in a slotted wall test section. To prevent balance fouling, 0.4 inches of material was removed from the aft end of the C4 body. This required that cavity/chamber pressures be measured so that the difference in drag due to the aft end modification could be taken into account by correcting to the test section static pressure. Critical dimensions and parameters for the NTF bodies, including these modifications, are provided in Table 1.

Testing these two geometrically scaled test articles in a fixed test section configuration has the advantage is that the mathematical model of the wall boundary condition and the corresponding parameters should not change. The disadvantage is that the potential for test-article-to-test-article variation is present, such as geometric and mounting differences.

To address item (2b) from above, the test section slots on both the floor and the ceiling which can be selectively closed with slot covers. The three configurations, shown schematically in Figure 3, chosen for use in this study maintain symmetry of the test section about the tunnel centerline. Advantages and disadvantages of this element of testing are opposite those discussed previously for geometric scaling. The advantage now is that one article can be examined in several test section configurations. This eliminates the test-article-to-test-article variation; instead, it is only necessary to match conditions between the test section configurations. The disadvantage is that for changes in ventilation, parameters of the mathematical model of the wall boundary condition change to correspond to the new physical constraint imposed by the boundary. This will also aid in the validation of the calibration process, since the calibration of the wall boundary condition is part of the modeling of the wall interference method.

To aid in inferences drawn from the validation test, the notions of severe testing are introduced. The more likely the test will demonstrate a difference between competing theories (discrimination) or between theory and reality (validation), the stronger the inference that can be made concerning the test (*i.e.,* placing the model in jeopardy of failure if it is indeed inadequate for a specified purpose). A technical definition of a severe test is presented by Mayo,[29,30] and further discussion of placing a model in jeopardy of failure is given by Box, Hunter, and Hunter.[31]

How then does severe testing impact the validation of wall interference correction models? As stated above, the desire is to test in regions where the wall interference model is forced to operate on the data to provide evidence of its adequacy. These regions were not well known in advance of the bodies-of-revolution test, since the TWICS process requires wall pressure data for the test article. In addition, there was some uncertainty regarding the appropriate form of the boundary condition and its corresponding parameter values. Testing parameters were chosen to force the case to differ as much as possible based on the following information. As discussed earlier, the TWICS methodology uses a constrained, linear, compressible model of the flow field potential, based on Prandtl-Glauert scaling; so, as transonic flow over the test article develops, it is expected that it will become increasingly difficult to correct the wind tunnel conditions to a corresponding free-air state; ultimately, the wind tunnel flow will be uncorrectable. Thus, the test becomes more severe as higher transonic Mach numbers are reached and the assumption of linear potential flow is violated.

For this study there are two severe tests that are constructed to ensure that differences occur:

1. Among cases: Combinations of various bodies-of-revolution in different test section ventilation settings, given in Table 2, are expected to produce different results. Additionally, for this particular study of TWICS, differences are still expected at higher transonic conditions even after wall interference corrections have been applied. This will aid in establishing the domain of applicability.

2. Among wall boundary condition models: The three ventilated wall boundary conditions, GSW, ISW, PW, given in Equations 3, 4, and 5, respectively, are the competing models and are expected to produce different results.

D. Summary and Results of the Bodies of Revolution Test

Several combinations of the bodies of revolution and ventilation configurations of the NTF discussed above were tested, as shown in Table 2. The test conditions, given in Table 3 for a stream temperature of 120F using air as the test medium, for this experiment were chosen to allow comparison of the bodies at a matched Reynolds number of 27×10^6 based on body length. Both bodies were tested on the test section centerline with angle-of-attack varying no more than 0.3° over three nominal settings near zero. No meaningful correlation of the drag coefficient was seen with either the incidence angle, the pitching moment coefficient, or the lift coefficient; thus, no correction of drag-due-to-lift was required. A 0.1 in. boundary-layer transition-strip of #180 (0.0035 in.) grit was placed at approximately 2 percent of the body length downstream of the nose, using established methods.[32–34] Transition was verified with sublimating chemicals on each body. Aerodynamic forces were measured using a six-component strain-gage balance, with a maximum axial force load of 125 lbs. Test article cavity and surface pressure measurements were acquired using a 15 psid ESP pressure transducer referenced to the plenum pressure.

All corrections except for wall interference were applied to the measured drag coefficient, $C_{D_{\text{meas}}}$. These corrections consisted of:

1. A drag coefficient increment due to cavity pressure, $\Delta C_{D_{\text{cav}}}$

2. A drag coefficient increment due empty test section buoyancy, $\Delta C_{D_{\text{etb}}}$

The drag coefficient uncorrected for wall interference, $C_{D_{\text{u}}}$, is then

$$C_{D_{\text{u}}} = C_{D_{\text{meas}}} + \Delta C_{D_{\text{cav}}} + \Delta C_{D_{\text{etb}}} \tag{9}$$

For details of these corrections, their development, and the uncertainty buildup, see Walker.[2,3]

For the remainder of this paper, C_D values for each body at a given Mach number are averaged over replicate sets of 9 data points to account for minor variations present during testing. This averaged drag coefficient is denoted as $\bar{C}_D$. A comparison of $\bar{\bar{C}}_{D_{\text{u}}}$ as a function of the test section calibrated Mach number, M_{TS}, is shown in Figure 4a for each of the four body/test section combinations given in Table 2. The uncertainty interval, shown as error bars, is determined by multiplying the standard deviation estimate by a coverage factor, in this case, 2. A coverage factor of 2 is a balance between typical values used in either exploratory or confirmatory analysis.

To highlight the relative differences of cases being compared, general trends of the data set are removed to create a residual scale comparison. The average of $\bar{\bar{C}}_{D_{\text{u}}}$ at each M_{TS} across the four validation cases shown in Figure 4a was subtracted from each case and is presented in Figure 4b. The uncertainty interval from each of the four cases was averaged and plotted about the axis. This figure shows that for $M_{\text{TS}} > 0.65$ the four validation cases are significantly different, yielding the validation test discussed in the next section.

E. The Resulting Validation Test

The four cases shown in Figure 4 constitute the validation test for wall-induced-blockage interference. The expectation is that a wall interference model would collapse the four cases within the uncertainty (after correction) at conditions for which the model assumptions are valid. The severity of the validation test is important for making inferences. Referring to Figure 4b, with respect to the uncertainty interval indicated, the test is not severe for $M_{\mathrm{TS}} < 0.65$. Post correction analysis for these Mach numbers will not necessarily indicate adequacy of the mathematical modeling; however, if the wall correction modeling introduces more disagreement among these four cases, especially above the estimated uncertainty, the wall interference model would be introducing error indicating that modeling errors are significant. For $M_{\mathrm{TS}} \geq 0.65$, the test is severe, and effective wall interference correction methodology would be expected to reduce the spread in the data.

The uncertainty interval becomes a test of whether the modeling errors are significant, for the first time allowing the uncertainty of wall-induced-blockage interference corrections to be quantitatively established. Residual-scale analysis can demonstrate modeling improvements even when the modeling error is significant.

III. Model Discrimination and Validation Analysis

Before the model discrimination and validation analysis were performed, the wall boundary condition parameters, K and B given in Equations 3-5, and their uncertainties were estimated using a calibration developed by Walker.[2,3] The calibration process involved determining values of the parameters that best fit the tared wall signature data from the C4 body in each of the three ventilation settings given in Table 2. Parameter estimation was performed for each of the three ventilated wall boundary conditions for each of the 12 Mach numbers shown in Table 3. Since the validation is performed across the four body/test section configurations, and the wall boundary condition calibration is performed within the test section configurations, the validation test was not compromised by the wall boundary condition calibration. The purpose of this section is to discuss the results of the application of the calibrated wall interference models to the data acquired on the bodies-of-revolution. The resulting corrected data is analyzed with respect to the model discrimination and validation tests discussed previously.

A. Final Correction Equation

The final correction equation for the drag coefficient is given by

$$C_{D_C} = (C_{D_{\mathrm{u}}} + \Delta C_{D_{\mathrm{cavw}}}) \cdot C_q + \Delta C_{D_{\mathrm{mib}}} \tag{10}$$

$$= C_{D_C}(M_\infty) = C_{D_C}(M_{\mathrm{TS}} + \Delta M) \tag{11}$$

where $\Delta C_{D_{\mathrm{cavw}}}$ is the drag coefficient correction due to the wall interference increment to static pressure in the cavity pressure correction, $C_q = q_{\mathrm{TS}}/q_\infty$ is the ratio test section indicated to wall interference corrected dynamic pressure, $\Delta C_{D_{\mathrm{mib}}}$ is the drag coefficient correction due to buoyancy induced by the solid blockage of the test article, M_∞ is the corrected free stream Mach number and ΔM is the wall interference correction to Mach number. Corrections were applied to the data, so that the following two analyses could be made:

1. Model discrimination: This is a comparison of C_{D_C} from each of three wall boundary conditions formulations. Its purpose is to show the similarity and differences associated with corrections applied using the ISW, PW, and GSW wall boundary condition models.

2. Model validation: This is a comparison of C_{D_C} of the four validation cases: C4 body in 2%, 4%, and 6% test sections and the C3 body in the 6% test section. The comparison is made for each of the three wall boundary condition formulations. Its purpose is to determine if the corrected data from the four independent cases are in agreement as would be expected if the wall interference correction method were perfect.

B. Model Discrimination Analysis

Having corrected the data for wall interference using each of the three ventilated wall boundary conditions, the model discrimination comparisons can be analyzed in the presence of uncertainty. Figure 5a shows the correction of the C4 body data for each of the three ventilated wall models. As discussed by Walker,[2,3]

a modification of the uncertainty was introduced here by removing fossilized (fixed) uncertainty due to calibration that was common to each of the three models, thus comparing the results of the three wall boundary conditions using only the relative uncertainty among them. The modified uncertainty is, as before, applied to each comparison case using a coverage factor of 2.

Figure 5b shows the residual scale comparisons with respect to the mean correction from the three models. The average modified uncertainty is applied about the zero axis. It is clear from these plots that the three boundary conditions models yield significantly, beyond what is explained by the uncertainty, different results, especially for Mach numbers above 0.7.

C. Validation Analysis

Figures 6-8 show the corrected drag coefficient (a) and relative drag coefficient (b) from the four body/test section configurations (validation cases) for each of the wall boundary condition models, ISW, PW, and GSW respectively, as a function of the corrected Mach number, M_∞. As before, the combined standard uncertainty for Figures 6a-8a is applied to the data using a coverage factor of 2. There are several important points to be made from the comparisons of the validation cases for each of the three wall boundary conditions:

1. While drag rise is evident in the results using the ISW model (Figure 6a), the free-stream Mach number at which it occurs is different for each case. Drag rise is defined here as $\partial \bar{\bar{C}}_D / \partial M > 0$, the onset of which is seen when $\partial \bar{\bar{C}}_D / \partial M = 0$.

2. With the exception of the C3 body in the 6% test section, the PW model (Figure 7a) does not show the onset of drag rise for corrected Mach numbers up to 0.987.

3. While the corrected drag data are not in complete agreement for the GSW model (Figure 8a), it is interesting to note that the onset of drag rise is consistently predicted to be in the interval $0.96 \leq M_{\mathrm{TS}} \leq 0.97$.

Figures 6b-8b show the residual scale comparisons with respect to the mean correction from the four validation cases. As before, the average uncertainty from the validation cases is applied about the zero axis. For the ISW model (Figure 6b):

1. For $M_{\mathrm{TS}} \approx M_\infty \leq 0.65$, the four validation cases agree to within the uncertainty.

2. As Mach number is increased, results from the cases with the most (C4 body, 2% test section) and least (C3 body, 6% test section) interference diverge from the mean in opposite directions.

For the PW model (Figure 7b):

1. For $M_{\mathrm{TS}} \approx M_\infty \leq 0.60$, the four validation cases approximately agree to within the uncertainty.

2. As Mach number is increased, results from the C3 body (6% test section) still diverge significantly from the mean with increasing Mach number as was seen with the ISW model.

3. While they are significantly different above a Mach number of 0.6, results among the C4 body cases agree much better than they did with the ISW model and are close to the estimated uncertainty.

For the GSW model (Figure 8b):

1. For $M_{\mathrm{TS}} \approx M_\infty \leq 0.65$, the four validation cases approximately agree to within the uncertainty.

2. While they are significantly different above a Mach number of 0.65, results for all cases agree much better than with either the ISW or PW models.

Figures 6-8 show that results from the GSW model agree much better than those from either the ISW or PW models, possibly indicating that each of the single parameter models are missing some essential physics of the problem. Further evidence is seen from the wall signature fits using each of the three wall boundary conditions. Figure 9 shows the normalized velocity distribution u/U_{TS} from both the tared data and the resulting TWICS fit along two representative pressure rows in the NTF (Figure 1) for each of the three boundary conditions. The circles and dash-dot line are from the centerline on the slotted floor (Row 3), and

the squares and solid line are from the centerline of the solid sidewall (Row 9). Figure 9a shows that while the calibrated ISW model is able to capture the signature on the solid sidewall, it misses both the peak and location of the slotted floor signature. As shown in Figure 9b, the calibrated PW model is able to capture the slotted floor signature but misses that of the solid sidewall. Figure 9c shows much better agreement from the GSW model with both the solid sidewall and slotted floor signatures. Given that this is an elliptical problem, it should be expected that the effects of both of the wall types need to be represented. While this is far from proving that the GSW model has the correct physical representation, it can be reasonably argued that the GSW is more representative of the data and physics than either the ISW or PW models–supporting the work of Everhart.[27] The GSW model has the advantage of simultaneously modeling the flow curvature (φ_{xn}) and flow pressure drop (φ_n) in the slots; whereas, the single parameter models force the pressure at the wall (φ_x) to be due to only the flow curvature (ISW) or pressure drop (PW) in the slots.

Even using the best of the three wall boundary conditions, the GSW model shown in Figure 8, the validation cases are still significantly different for $M_\infty \geq 0.60$; however, the variation among the four validation cases is greatly reduced at the higher subsonic and transonic Mach numbers. For $M_\infty \leq 0.60$ the dispersion across the four cases appears to have been reduced, but the four cases were not significantly different from the mean before wall interference corrections were applied. In other words, it was not difficult for the wall interference model to account for variation that was not significant to begin with—the test of the wall interference correction process was not severe at the lowest Mach numbers.

This analysis shows that even the best of the three wall boundary condition models, GSW, does not explain all of the variation present across the four validation cases, at least to within the estimated correction process variation. Even if the correction process uncertainty estimate is incorrect by a factor of 2, it would not explain all the variation present across these four cases for $M_\infty \geq 0.80$.

IV. Summary

A process for the statistical validation of wall interference methods has been developed. This process allows the detection of modeling or implementation deficiencies using comparisons of independently generated cases, which would reasonably be expected to yield the same result after application of the process, to within the estimated uncertainty in the process used to generate the final results. This method was applied to the NTF implementation of the TWICS code for blockage and induced buoyancy corrections in longitudinally slotted test sections. For the first time, the uncertainty of wall-induced-blockage interference corrections was quantitatively established.

Calibrated versions of three historical linear models of the ventilated wall boundary condition were compared over 4 test case drag polars obtained at matching test conditions on scaled bodies of revolution. The test cases included a larger body in the 2%,4% and 6% wall ventilation configurations of the NTF and a smaller body, approximately half the volume, in the 6% wall ventilation configuration. Although none of the implementations of these models were validated to within the estimated uncertainty for $M_\infty > 0.60$, the General Slotted Wall (GSW) model was found to be the best of the three based on the following:

1. The representation of the tared wall signatures,
2. The approximate alignment of the onset of drag rise in the final corrected drag coefficient, and
3. The best overall agreement of the four validation cases.

Both the Ideal Slotted Wall (ISW) and Porous Wall (PW) boundary conditions were found to be lacking critical modeling terms, preventing an adequate capturing of the known flow physics behavior.

Acknowledgments

The author gratefully acknowledges the contributions of the following individuals to this test program: Venkit Iyer, TWICS-NTF implementation; David Kuhl, wall pressure data quality analyst; Jerry Adcock, NTF test engineer; Allen Kilgore, NTF facility manager; and Laurence Leavitt and Dr. Richard Wahls, head and assistant head Configuration Aerodynamics Branch, respectively. In addition, the author thanks Drs. Michael Hemsch, Joel Everhart, and Richard Barnwell for the many discussions it took to make this study possible. The author also thanks Dr. James Luckring for his extensive review of this paper.

References

[1]Walker, E., "Measuring Wall Interference Correction Accuracy: An Overview of the NTF Program (Invited)," January 5-8 2004, *Presented at the 42nd AIAA Aerospace Sciences Meeting and Exhibit*, AIAA Paper 2004-0770.

[2]Walker, E., *Statistical Calibration and Validation of a Homogeneous Ventilated Wall-Interference Correction Method for the National Transonic Facility*, Ph.D. thesis, Virginia Polytechnic Institute and State University, October 2005, Available electronically at http://scholar.lib.vt.edu/theses/available/etd-10272005-165559/.

[3]Walker, E., "Statistical Calibration and Validation of a Homogeneous Ventilated Wall-Interference Correction Method for the National Transonic Facility," NASA/TP 2005-213947, 2005, Available electronically at http://ntrs.nasa.gov.

[4]Hemsch, M., "Development and Status of Data Quality Assurance Program at NASA Langley Research Center–Toward National Standards," AIAA Paper 96-2214, 1996, *Presented at the 19th AIAA Advanced Measurement and Ground Testing Technology Conference, New Orleans, LA.*

[5]Hemsch, M., Grubb, J., Krieger, W., and Cler, D., "Langley Wind Tunnel Data Quality Assurance-Check Standard Results," AIAA Paper 2000-2201, 2000.

[6]Fuller, D., Gloss, B., and Nystrom, D., "Guide for Users of the National Transonic Facility," NASA TM 83124, July 1981.

[7]Ulbrich, N. and Lo, C., "A Wall Interference Assessment/Correction System," Semi-Annual Report #1, The University of Tennessee Space Institute, December 1991.

[8]Ulbrich, N., Lo, C., and Steinle, Jr., F., "Blockage Correction in Three-Dimensional Wind Tunnel Testing Based on the Wall Signature Method," July 6-8 1992, *Presented at the AIAA 17th Aerospace Ground Testing Conference*, AIAA Paper 92-3925.

[9]Ulbrich, N. and Steinle, Jr., F., "Real-Time Wall Interference Calculation in Three-Dimensional Subsonic Wind Tunnel Testing," January 10-13 1994, *Presented at the 32nd Aerospace Sciences Meeting and Exhibit*, AIAA Paper 94-0771.

[10]Ulbrich, N. and Steinle, Jr., F., "Semispan Model Wall Interference Prediction Based on the Wall Signature Method," January 9-12 1995, *Presented at the 33rd Aerospace Sciences Meeting and Exhibit*, AIAA Paper 95-0793.

[11]Ulbrich, N. and Boone, A., "Real-Time Wall Interference Correction System of the 12FT Pressure Wind Tunnel," January 12-15 1998, *Presented at the 36th Aerospace Sciences Meeting and Exhibit*, AIAA Paper 98-0707.

[12]Ulbrich, N., "The Real-Time Wall Interference Correction System of the NASA Ames 12-Foot Pressure Tunnel," NASA CR 1998-208537, 1998.

[13]Ulbrich, N. and Boone, A., "Determination of the Wall Boundary Condition of the NASA Ames 11FT Transonic Wind Tunnel," January 8-11 2001, *Presented at the 39th Aerospace Sciences Meeting and Exhibit*, AIAA Paper 2001-1112.

[14]Ulbrich, N. and Boone, A., "Direct Validation of the Wall Interference Correction System of the Ames 11-Foot Transonic Wind Tunnel," May 2003, NASA/TM-2003-212268.

[15]Hackett, J. and Wilsden, D., "Determination of Low Speed Wake Blockage Corrections Via Tunnel Wall Static Pressure Measurements," *Wind Tunnel Design and Testing Techniques*, March 1976, AGARD-CP-174. *Presented to the AGARD Fluid Dynamics Panel Symposium on Wind Tunnel Design and Testing Techniques: London, England, 6-8 October 1975.*

[16]Hackett, J. and Boles, R., "Wake Blockage Corrections and Ground Effect Testing in Closed Wind Tunnels," *Journal of Aircraft*, Vol. 13, No. 8, August 1976, pp. 597–604.

[17]Hackett, J. and Wilsden, D., "Estimation of Wind Tunnel Blockage from Wall Pressure Signatures: A Review of Recent Work at Lockheed-Georgia," AIAA Paper 78-828, April 1978.

[18]Hackett, J., Wilsden, D., and Lilley, D., "Estimation of Tunnel Blockage from Wall Pressure Signatures: A Review and Data Correlation," NASA CR 15224, March 1979.

[19]Hackett, J., Wilsden, D., and Stevens, W., "A Review of the "Wall Pressure Signature" and Other Tunnel Constraint Correction Methods for High Angle-of-Attack Tests," AGARD R 692, February 1981, *Presented to the AGARD Fluid Dynamics Panel Round Table Discussion on Wind Tunnel Corrections for High Angle-of-Attack Models: Munich, FRG, 8 May 1980.*

[20]Hackett, J., Sampath, S., and Phillips, C., "Determination of Wind Tunnel Constraint Effects by a Unified Pressure Signature Method. Part I: Applications to Winged Configurations," NASA CR 166186, June 1981.

[21]Hackett, J., Sampath, S., and Phillips, C., "Determination of Wind Tunnel Constraint Effects by a Unified Pressure Signature Method. Part II: Applications to Jet-In-Crossflow Cases," NASA CR 166187, June 1981.

[22]Hackett, J., "Living with Solid-Walled Wind Tunnels," AIAA 82-0583, March 1982, *Presented at the AIAA 12th Aerodynamic Testing Conference, March 22-24, 1982, Williamsburg, VA.*

[23]Iyer, V., Everhart, J., Bir, P., and Ulbrich, N., "Implementation of the WICS Wall Interference Correction System at the National Transonic Facility," June 19-22 2000, *Presented at the 21st AIAA Aerodynamic Measurement Technology and Ground Testing Conference, Denver, CO*, AIAA Paper 2000-2383.

[24]Iyer, V. and Everhart, J., "Application of Pressure-Based Wall Correction Methods to Two NASA Langley Wind Tunnels," June 11-14 2001, *Presented at the 19th AIAA Applied Aerodynamics Conference, Anaheim, CA*, AIAA Paper 2001-2472.

[25]Ulbrich, N., "The Representation of Wind Tunnel Model Blockage Effects Using Point Doublets," January 14-17 2002, *Presented at the 40th Aerospace Sciences Meeting and Exhibit*, AIAA Paper 2002-0880.

[26]Pindzola, M. and Lo, C., "Boundary Interference at Subsonic Speeds in Wind Tunnels with Ventilated Walls," Tech. rep., May 1969, AEDC-TR-69-47, U.S. Air Force.

[27]Everhart, J., *Theoretical and Experimental Studies of the Transonic Flow Field and Associated Boundary Conditions Near a Longitudinally-Slotted Wind-Tunnel Wall*, Ph.D. thesis, The George Washington University, February 14, 1988, Available as NASA TM-103381.

[28]Couch, L. and Brooks, Jr., C., "Effect of Blockage Ratio on Drag and Pressure Distributions for Bodies of Revolution at Transonic Speeds," NASA-TN D-7331, November 1973.

[29]Mayo, D., *Error and the Growth of Experimental Knowledge*, The University of Chicago Press, 1996.

[30]Mayo, D. and Spanos, A., "A Post-Data Interpretation of Neyman-Pearson Methods Based on a Conception of Severe Testing," Tech. rep., Measurements in Physics and Economics Discussion Paper Series, London School of Economics, Center for Philosophy of Natural and Social Science, 2000.

[31]Box, G., Hunter, W., and Hunter, J., *Statistics for Experimenters: An Introduction to Design, Data Analysis, and Model Building*, John Wiley and Sons, New York, 1978.

[32]Chapman, D. and Rubesin, M., "Temperature and Velocity Profiles in the Compressible Laminar Boundary Layer with Arbitrary Distribution of Surface Temperature," *Journal of the Aeronautical Sciences*, Vol. 16, No. 9, September 1949, pp. 547–579.

[33]Braslow, A. and Knox, E., "Simplified method for determination of critical height of distributed roughness particles for boundary-layer transition at Mach numbers from 0 to 5," NACA-TN 4363, 1958.

[34]Braslow, A., Hicks, R., and Harris, Jr., R., "Use of Grit-Type Boundary-Layer-Transition Trips on Wind-Tunnel Models," NASA-TN D-3579, 1966.

Table 1. Test Article Description

Body	L(in)	$d_{\max}$(in)	$L/d_{\max}$	S(ft^2)	S/C	A_{base}(ft^2)	V(ft^3)	V/S(ft)
C3	55.62	5.8548	9.50	0.18696	0.00278	0.01250	0.6041	3.231
C4	68.53	7.2554	9.45	0.28711	0.00427	0.02485	1.1489	4.002

Table 2. List of Test Data by Unit Reynolds Number and Configuration

Body	TS	Re/ft($\times 10^6$)	Replicates
C4	2%	4.7	2
	4%	4.7	2
	6%	4.7	2
C3	6%	5.8	1

Table 3. Nominal Test Conditions

Re/ft:	4.7×10^6		5.8×10^6	
M_{TS}	p_0(psi)	q(psf)	p_0(psi)	q(psf)
0.400	29.9	432	37.0	535
0.500	24.9	529	30.8	654
0.600	21.7	618	26.8	765
0.700	19.6	699	24.3	865
0.800	18.2	772	22.6	955
0.850	17.7	805	21.9	996
0.900	17.3	836	21.4	1034
0.925	17.1	851	21.2	1053
0.950	17.0	865	21.0	1070
0.960	16.9	870	20.9	1077
0.970	16.9	876	20.9	1083
0.980	16.8	881	20.8	1090

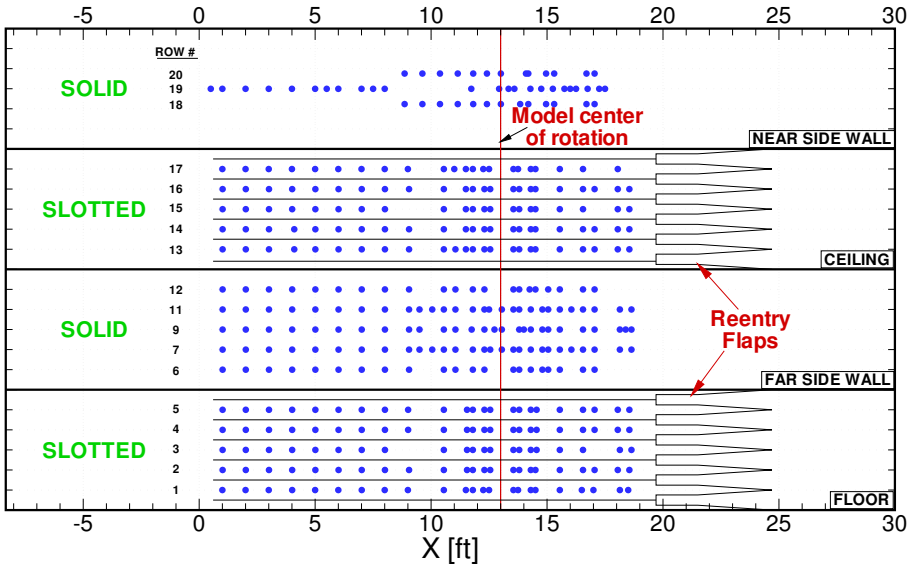

Figure 1. Wall Orifice Layout for NTF

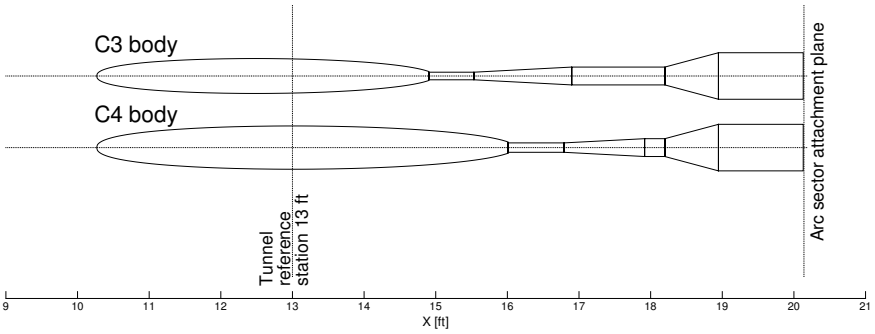

Figure 2. Bodies of Revolution/Sting Assembly

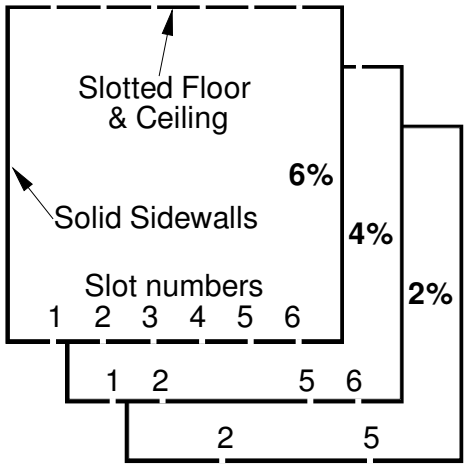

Figure 3. NTF slot configurations

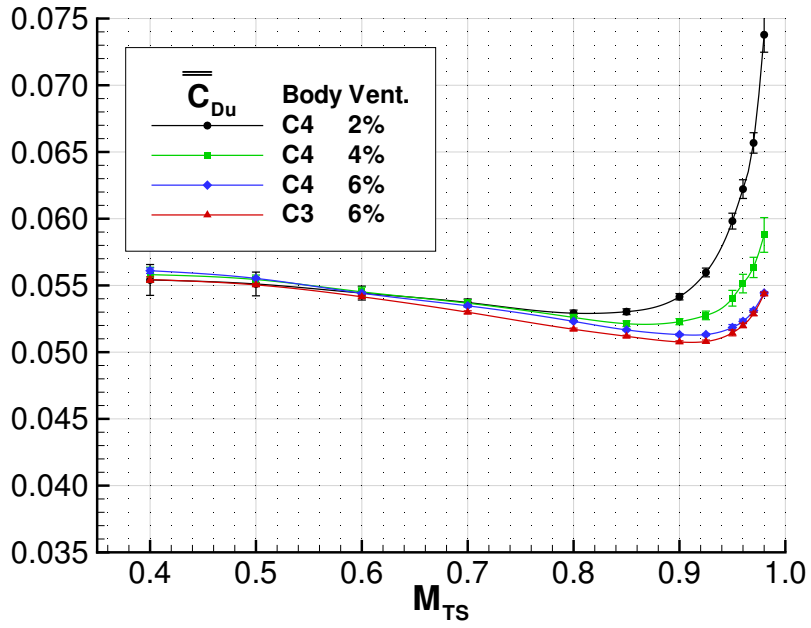

(a) Average Drag Coefficient

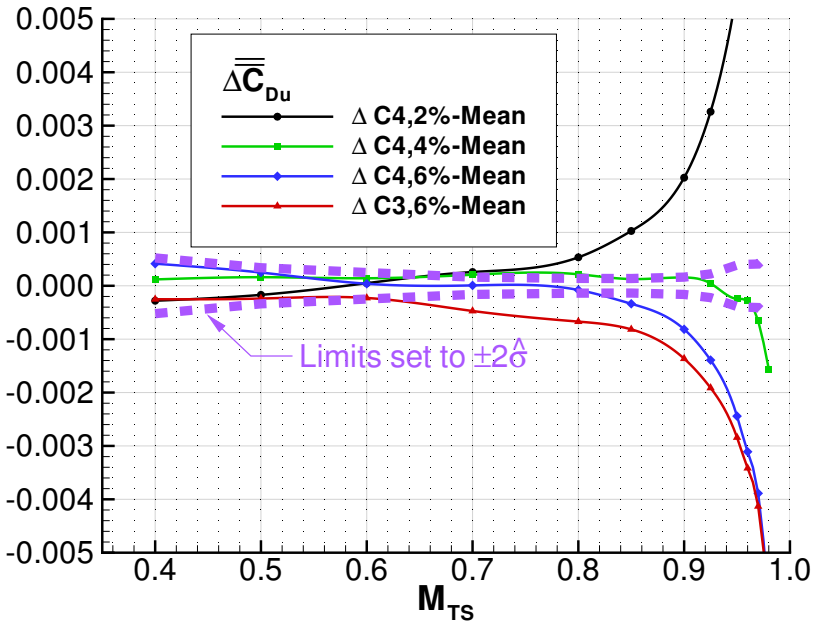

(b) Relative Drag Coefficient (Residual Scale)

Figure 4. Comparison of $\bar{\bar{C}}_{D_u}$ with Uncertainty. $Re_L = 27 \times 10^6$.

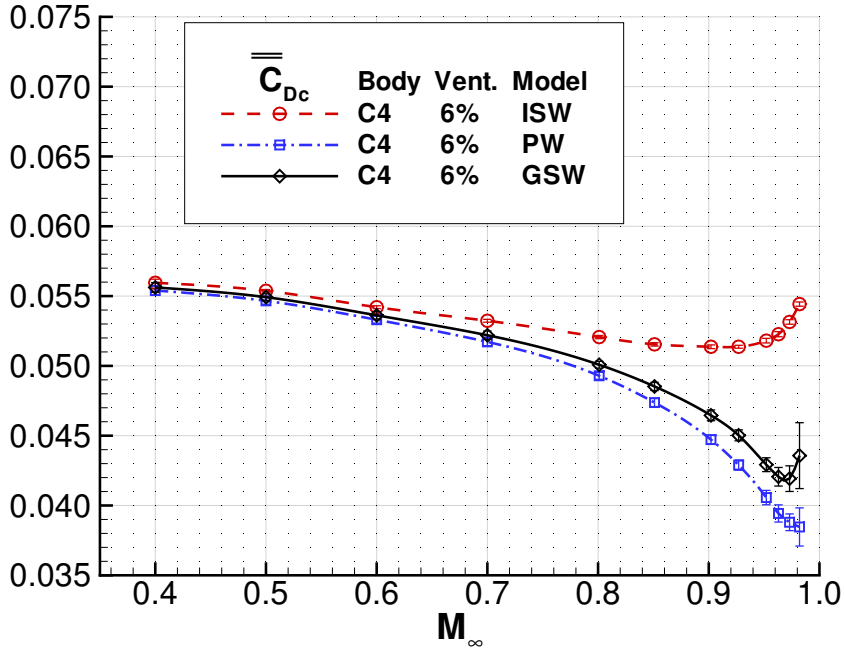

(a) Average Corrected Drag Coefficient

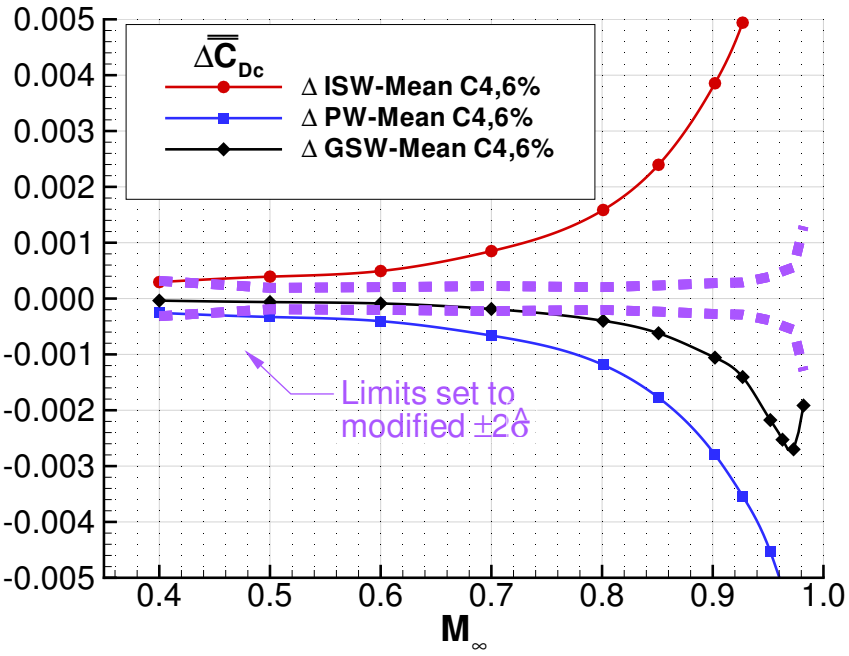

(b) Relative Corrected Drag Coefficient (Residual Scale)

Figure 5. Wall Boundary Condition Model Discrimination Comparison, C4 body, 6% Test Section

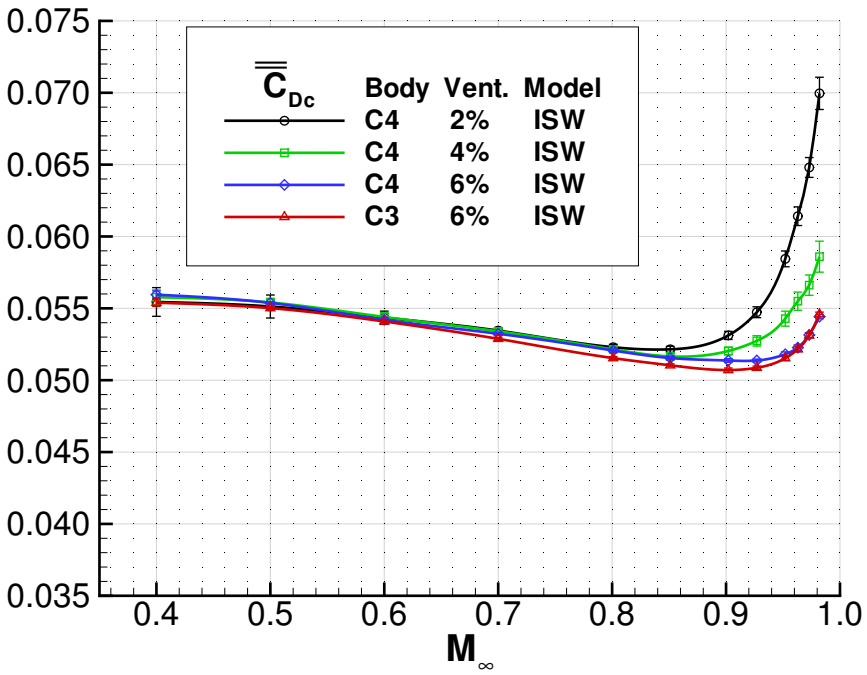

(a) Average Corrected Drag Coefficient

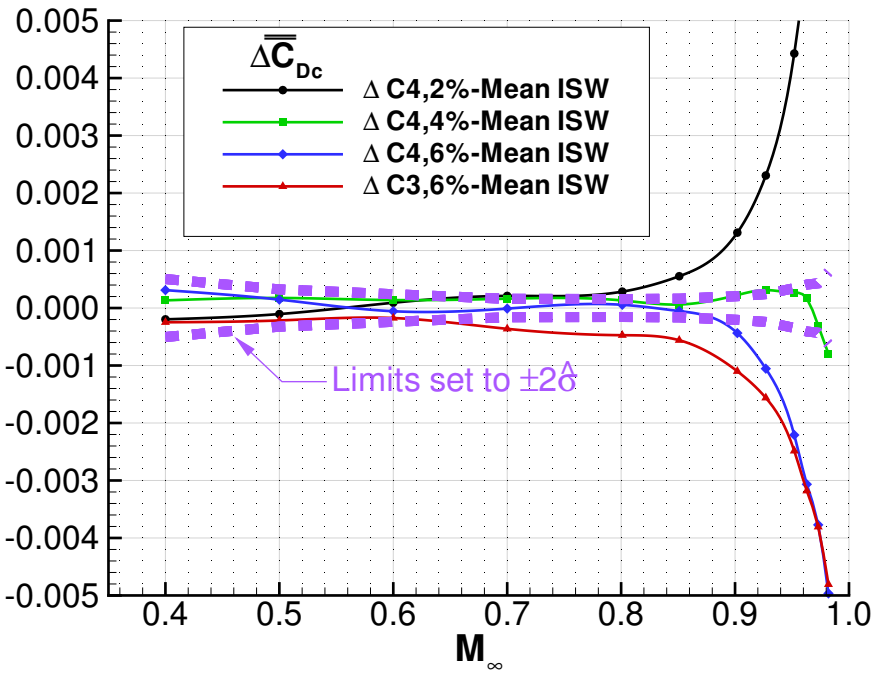

(b) Relative Corrected Drag Coefficient (Residual Scale)

Figure 6. Validation Comparison using ISW model

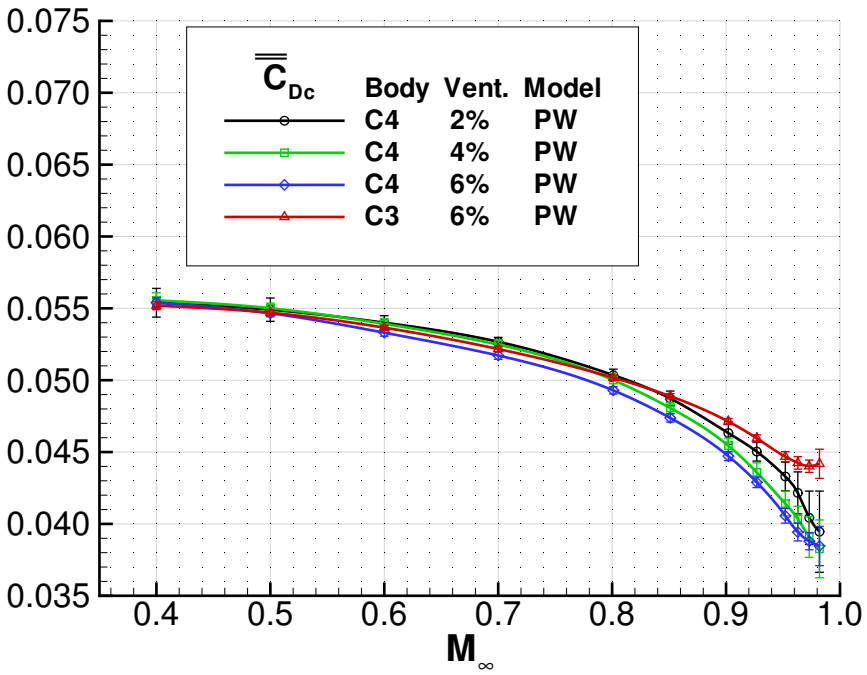

(a) Average Corrected Drag Coefficient

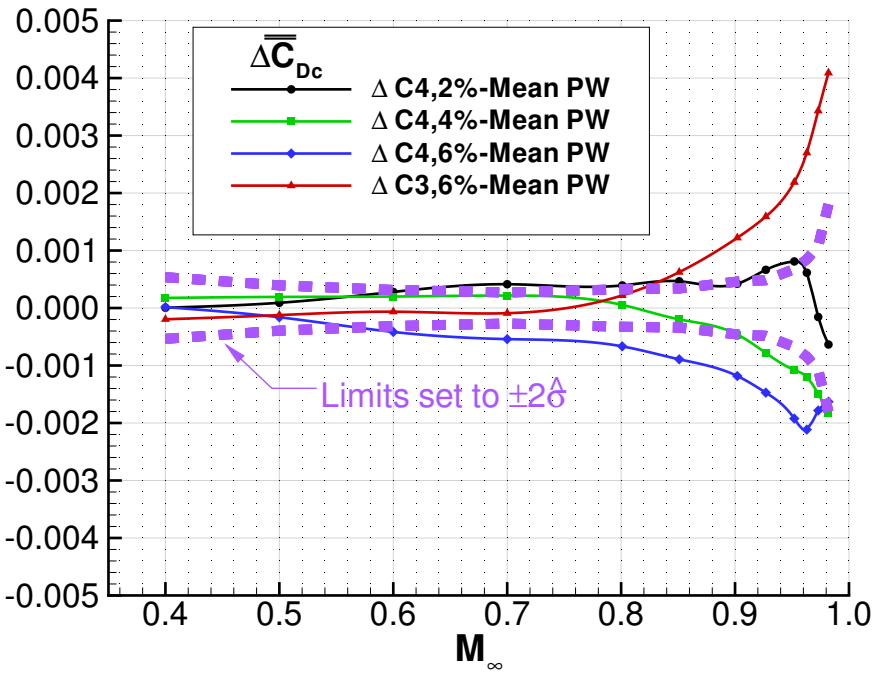

(b) Relative Corrected Drag Coefficient (Residual Scale)

Figure 7. Validation Comparison using PW model

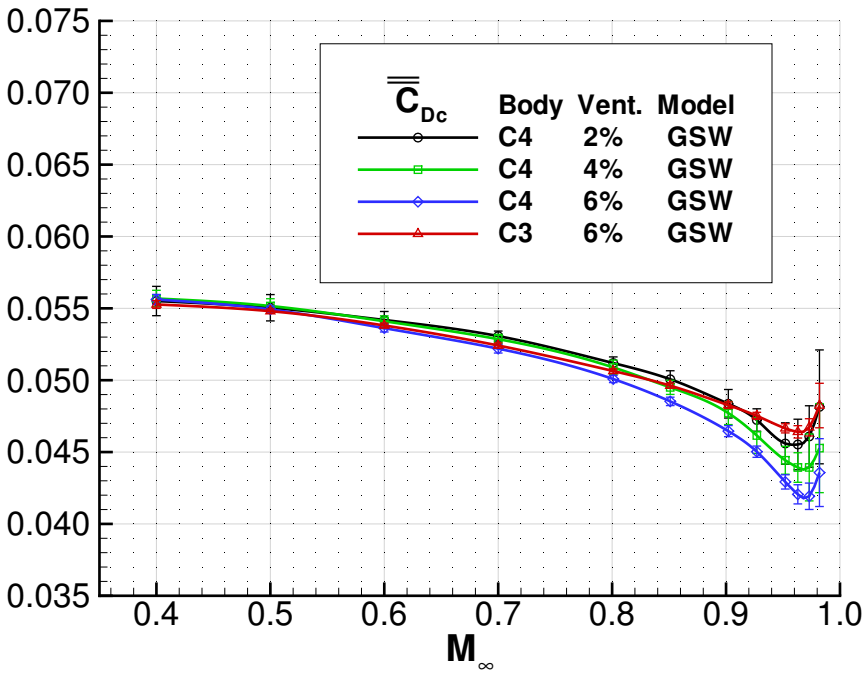

(a) Average Corrected Drag Coefficient

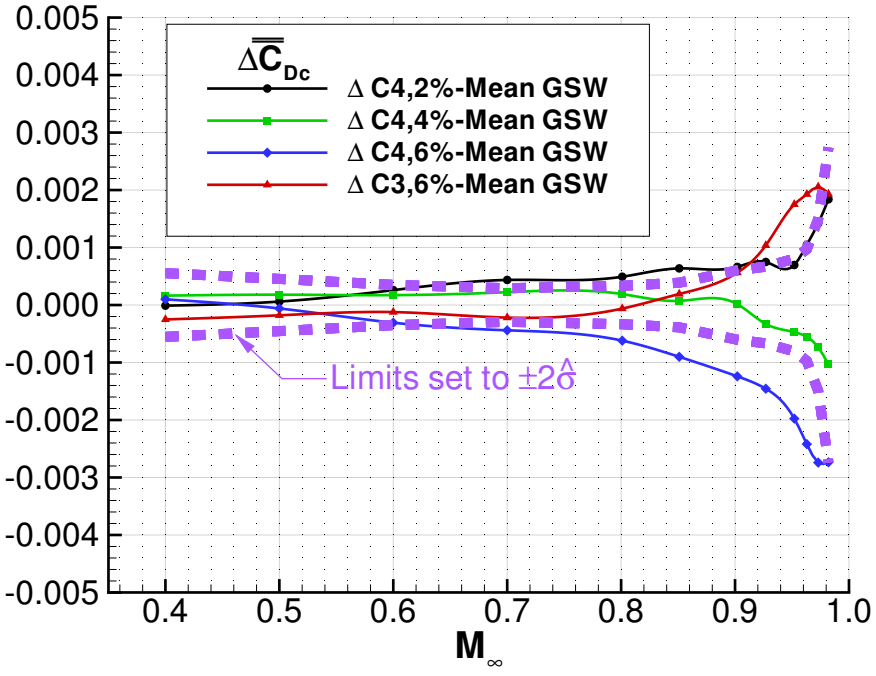

(b) Relative Corrected Drag Coefficient (Residual Scale)

Figure 8. Validation Comparison using GSW model

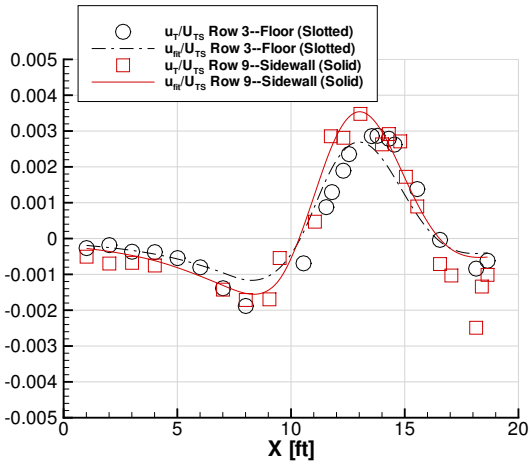

(a) ISW

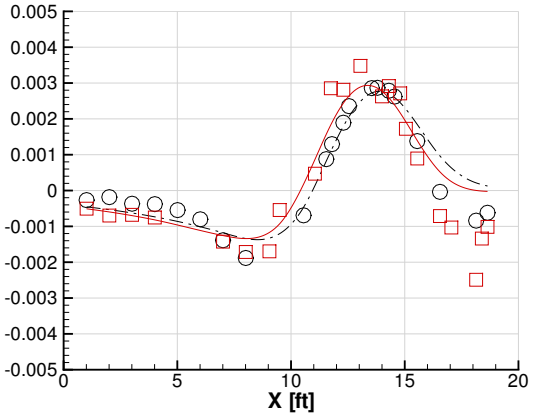

(b) PW

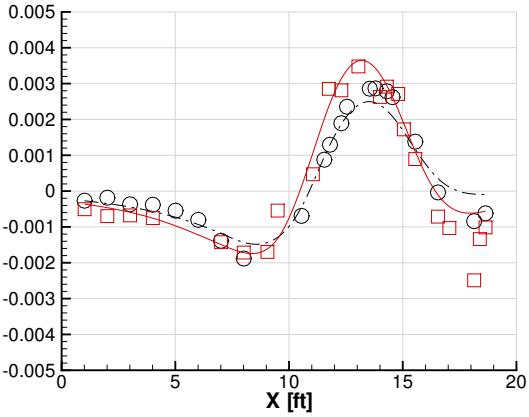

(c) GSW

Figure 9. Wall Signature Fits, C4 body, 6% Test Section, $M = 0.7$